

***p*-Band Engineering in Artificial Electronic Lattices**M. R. Slot,<sup>1,‡</sup> S. N. Kempkes,<sup>2,‡</sup> E. J. Knol,<sup>3</sup> W. M. J. van Weerdenburg,<sup>3</sup> J. J. van den Broeke,<sup>2</sup>  
D. Wegner,<sup>3</sup> D. Vanmaekelbergh,<sup>1</sup> A. A. Khajetoorians,<sup>3</sup> C. Morais Smith,<sup>2,\*</sup> and I. Swart<sup>1,†</sup><sup>1</sup>*Debye Institute for Nanomaterials Science, Utrecht University, Princetonplein 1, Utrecht 3584 CC, Netherlands*<sup>2</sup>*Institute for Theoretical Physics, Utrecht University, Princetonplein 5, Utrecht 3584 CC, Netherlands*<sup>3</sup>*Institute for Molecules and Materials, Radboud University, Heyendaalseweg 135, Nijmegen 6525 AJ, Netherlands*

(Received 19 September 2018; revised manuscript received 21 November 2018; published 16 January 2019)

Artificial electronic lattices, created atom by atom in a scanning tunneling microscope, have emerged as a highly tunable platform to realize and characterize the lowest-energy bands of novel lattice geometries. Here, we show that artificial electronic lattices can be tailored to exhibit higher-energy bands. We study *p*-like bands in fourfold and threefold rotationally symmetric lattices. In addition, we show how an anisotropic design can be used to lift the degeneracy between  $p_x$ - and  $p_y$ -like bands. The experimental measurements are corroborated by muffin-tin and tight-binding calculations. The approach to engineer higher-energy electronic bands in artificial quantum systems introduced here enables the realization of complex band structures from the bottom up.

DOI: [10.1103/PhysRevX.9.011009](https://doi.org/10.1103/PhysRevX.9.011009)

Subject Areas: Condensed Matter Physics

Bands composed of orbitals beyond *s* type play a key role for the electronic and magnetic properties of materials. Orbitals are characterized by the shape of the wave function, establishing a degree of freedom for the electrons in addition to spin and charge [1]. Higher orbitals (i.e., beyond *s* type) can give rise to interesting band structures, such as a Dirac cone and flatband for the *p*-orbital bands of a honeycomb lattice [2–4]. In addition, colossal magnetoresistance of several transition-metal oxides is related to the *d*-orbital bands in these systems [1]. In the presence of interactions, the nodal character of bosons in a *p*-band condensate [5–8] or of the superconducting order parameter in unconventional superconductors [9–12] leads to interesting broken-symmetry quantum phases and novel quantum effects.

Generally, the term “orbitals” refers to the nodal structure of the wave functions at the lowest (*s*) and higher (*p*, *d*, etc.) energies, which is equivalent to the nodal structure of atomic orbitals. More specifically, *s* orbitals in a lattice yield an either positive or negative wave-function amplitude at the lattice sites. In contrast, *p* orbitals alternate from a positive contribution between lattice sites via a node at the

site itself to a negative contribution on the other side. Bands originating from these *p* orbitals, so-called *p*-like bands, were studied in optical [5–8,13–15], photonic [16,17], and polariton lattices [18–20].

The manipulation capability of the low-temperature scanning tunneling microscope (STM) has been used to create atomically precise structures. This allows one to precisely control the electronic and spin coupling between atoms [21–26]. For artificial electronic systems, periodic (e.g., honeycomb, Lieb, checkerboard [27–30]) and non-periodic (quasicrystalline Penrose tiling and Sierpiński fractals [31,32]) geometries, as well as topologically non-trivial 1D chains [28,33], have been made. However, all of the experiments on electronic lattices focused on the lowest-energy bands, derived from *s*-like orbitals at the artificial-atom sites. In Ref. [34], Ma *et al.* pointed out that the higher-energy bands found for the Lieb lattice in Ref. [29] are well described by *p*-like bands, supported by a tight-binding model and plane-wave calculations.

Here, we first experimentally identify *p*-like bands in a fourfold rotationally symmetric Lieb lattice in which all sites host degenerate  $p_x$ - and  $p_y$ -like orbitals, by comparing the observed spatially dependent local density of states (LDOS) with muffin-tin calculations. Because the artificial atoms are two dimensional, there are only two *p*-like orbitals centered on each site, instead of three for real atoms. Then, we engineer a Lieb lattice in which the *p* degeneracy at the edge sites is broken, resulting in a separate  $p_x$ -like ( $p_y$ -like) orbital at the *x* (*y*) edge site in the energy range of interest. Next, by introducing an asymmetry in the lattice, we are able to lift the energy degeneracy of the remaining  $p_x$ - and  $p_y$ -like orbitals and

\*Corresponding author.

C.deMoraisSmith@uu.nl

†Corresponding author.

I.Swart@uu.nl

‡These authors contributed equally to this work.

Published by the American Physical Society under the terms of the [Creative Commons Attribution 4.0 International license](https://creativecommons.org/licenses/by/4.0/). Further distribution of this work must maintain attribution to the author(s) and the published article's title, journal citation, and DOI.

independently access these different degrees of freedom upon tuning the energy. Finally, to illustrate that the  $p$ -like band description is also applicable to systems with other symmetries, we investigate  $p$ -like bands in the threefold rotationally symmetric honeycomb lattice.

The electronic lattices are realized and characterized in two low-temperature STMs, located in Utrecht and Nijmegen (both Scienta Omicron LT-STM,  $T = 4.5$  K), in ultrahigh vacuum ( $p \approx 10^{-10}$  mbar). Carbon monoxide (CO) molecules are leaked into the chamber and adsorbed onto a cold Cu(111) single crystal in the STM, cleaned by sputtering and annealing cycles, such that the surface coverage was approximately 0.3 molecules per  $\text{nm}^2$ . A Cu-coated tungsten or platinum-iridium tip, prepared by gentle contact with the Cu(111) surface, is used for both the assembly and the characterization of the lattices. The CO molecules act as repulsive scatterers for the surface-state electrons of Cu(111) [35]. By positioning the CO molecules with atomic precision using the STM tip [36–38], the electrons at the surface of the Cu(111) crystal are confined to the regions in between the molecules, leading to the formation of an electronic lattice. In this manner, the confined 2D electron gas (2DEG) at the surface is patterned to form “artificial atoms” with a specific size—and thus on-site energy—and a tunable coupling between them. We characterize the nodal plane character of the wave function by mapping the LDOS at constant height at various energies. We utilize a lock-in technique and apply a modulation to the sample bias (modulation amplitude 5–20 mV rms, frequencies 273 and 4321 Hz). As evidenced by previous work [29,32], the muffin-tin model without many-body interactions yields a good description of the electronic band structure of artificial lattices generated by CO molecules on a Cu(111) surface. The muffin-tin calculations model the CO molecules by a circular repulsive potential with a radius  $r = 0.3$  nm and height of  $V_{\text{CO}} = 0.9$  eV in the Schrödinger equation for the 2DEG [29,39]. Not only the LDOS  $|\Psi|^2$  is calculated, but also the sign of the contributing wave functions  $\Psi$  is extracted. The results are further corroborated by single-particle tight-binding calculations, which model the artificial-lattice geometry with the appropriate orbitals at the artificial-atom sites [see Supplemental Material (SM) [40]].

First, we describe higher-orbital bands in a lattice with a fourfold rotational symmetry. For this purpose, we chose the Lieb lattice, which is a square-depleted lattice consisting of three (artificial) atoms (green) in a unit cell (blue dashed box) [41], as illustrated in Fig. 1(a). With three sites per unit cell, this lattice provides more flexibility than a square lattice. The three inequivalent artificial-atom sites consist of one corner site (1) and two edge sites (2 and 3). The size of the unit cell is chosen to be  $6\sqrt{3}a \times 10a \approx 2.66 \times 2.56 \text{ nm}^2$ , where  $a = 0.256$  nm is the Cu(111) nearest-neighbor distance (see SM [40]). This electronic lattice is realized by an array of CO molecules

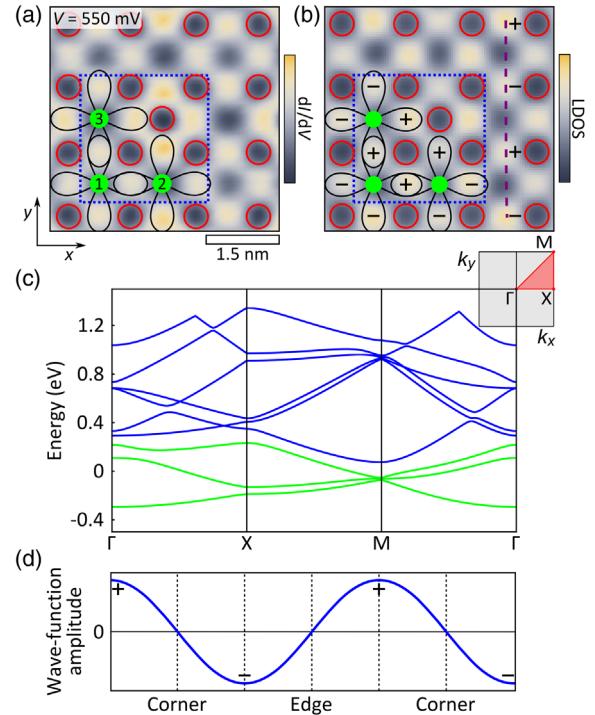


FIG. 1. (a) Differential-conductance map acquired at  $V = 550$  mV above a Lieb lattice, shown for part of the lattice. Images of the entire lattice can be found in the SM [40]. The unit cell (blue dashed box) contains three artificial-atom sites (green): one corner site (1) and two edge sites (2 and 3). The sites are generated by the configuration of CO molecules on a Cu(111) surface indicated by the red contours. The  $p$ -like orbitals in the unit cell are outlined by a black contour. The map was acquired at  $+110$  pm with respect to the set point  $I_{\text{set}} = 1$  nA,  $V_{\text{set}} = 50$  mV, with a bias modulation  $V_{\text{rms}} = 20$  mV. (b) LDOS map for the same energy simulated using the muffin-tin model. The  $p$ -like orbitals and the sign of the wave function are indicated in black. (c) Band structure along the high symmetry directions of the Brillouin zone (see inset) as calculated by a muffin-tin approach. The three lowest  $s$ -like bands are indicated in green, the six  $p$ -orbital bands in blue. (d) Bloch-type wave function along the purple dashed line in the muffin-tin simulation in (b). The wave function exhibits a positive maximum or negative minimum between the sites, while it is zero at the artificial-atom sites (corner and edges).

(red circles) on Cu(111), which acts as a repulsive potential and confines the electrons to the sites of the Lieb lattice [29,42]. At low energies  $E < 200$  meV, there are two bands exhibiting a Dirac cone at the corners of the Brillouin zone intersected by a third band [cf. green curves in Fig. 1(c)]. These bands have been observed experimentally and are well described by a tight-binding model using  $s$  orbitals at the artificial-atom sites [28,29].

Figure 1(a) shows a differential-conductance map acquired at a higher energy,  $V = 550$  mV. The map shows the central plaquette of a Lieb lattice of  $5 \times 5$  unit cells (see SM [40]). We observe that the artificial-atom sites (green) exhibit nodes in the LDOS, while there is an enhanced LDOS between the sites. This is in agreement with the

result from muffin-tin calculations [see Fig. 1(b)]. The nodal pattern corresponds to that of *p*-like orbitals, indicated schematically by black contours. These two-dimensional *p* orbitals consist of degenerate  $p_x$ - and  $p_y$ -like states, which extend between the sites to overlap with  $p_{x,y}$  states localized on a neighboring site. The variations in LDOS maxima between dangling and overlapping *p*-like orbitals can be attributed to differences in confinement (see SM [40]). We calculate the band structure of the Lieb lattice in the energy range  $-0.5 < E < 1.4$  eV using the muffin-tin model, as shown in Fig. 1(c). For  $-300 < E < 200$  meV, we obtain the three previously described lowest-energy bands (green). At higher energies,  $E > 200$  meV, additional bands are predicted (blue). To study the nature of the bands in more detail, we extract the wave-function amplitudes from the muffin-tin calculations. Figure 1(d) shows the value of the wave function along the purple line indicated in Fig. 1(b). Note that the amplitude of the wave function changes sign at the positions of the artificial atoms. In between these sites, it is either positive or negative. This corresponds to overlap of lobes with the same sign, i.e., a bonding combination of *p*-like orbitals on adjacent sites, as indicated in Fig. 1(b). Since there are two artificial atoms per unit cell along the *x* and *y* direction, the periodicity of the wave in Fig. 1(d) is the same as that of the unit cell. Thus, the muffin-tin calculations confirm the typical *p*-like character of the wave functions. A similar analysis of the lower-energy bands shows that the associated wave functions have *s*-like character (see SM [40]). If the energy is increased further, antibonding  $p_\pi$ -like and higher-orbital bands occur (see calculations in SM [40]).

Next, we alter the design of the Lieb lattice for two purposes. First, we shift the *p* bands down towards the Fermi energy, where the surface state of Cu(111) has a free-electron-like dispersion. Close to the Fermi energy the COs are more effective at confining the surface-state electrons and the influence of the bulk is minimized. We achieve this by increasing the size of the artificial-atom sites [27], reducing the confinement of the electrons. Second, we lift the degeneracy of the  $p_x$ - and  $p_y$ -like orbitals at the same edge sites by adding additional CO molecules, such that the dangling orbital is pushed to much higher energy. In Fig. 2(a), we show a differential-conductance map of this modified Lieb-like lattice with larger unit cells. The unit cell with size  $14a \times 8\sqrt{3}a \approx 3.58 \times 3.55$  nm<sup>2</sup> is indicated by a dashed blue box. It contains 12 CO molecules (encircled in red). Note that compared to the lattice discussed above, the edge sites in this design are more confined in the direction perpendicular to the line connecting two corner sites. As a guide to the eye, the locations of the artificial atoms are indicated in green and the *p*-like orbitals are outlined in black. For  $-300 < E < -100$  meV, the *s*-like bands were reproduced (see SM [40]). The differential-conductance map shown in Fig. 2(a) was acquired at  $V = 70$  mV. Note that there are nodes at the

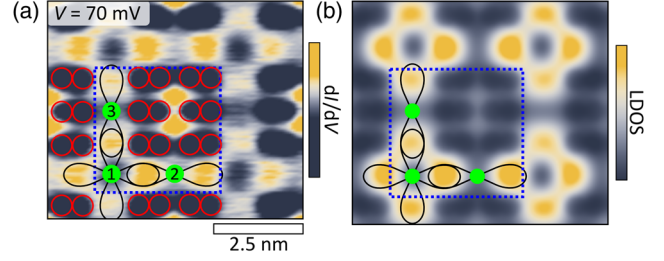


FIG. 2. (a) Differential-conductance map above a symmetric Lieb-like lattice acquired at  $V = 70$  mV, shown for part of the lattice (see SM [40] for entire lattice). The CO molecules are encircled in red and  $p_x$ - and  $p_y$ -like orbitals (black) are indicated in one unit cell (blue dashed box). The map was acquired after stabilization at  $I_{\text{set}} = 1$  nA,  $V_{\text{set}} = 70$  mV, with a bias modulation  $V_{\text{rms}} = 10$  mV. (b) LDOS map for the same energy simulated using the muffin-tin model.

positions of the artificial atoms. The corner sites (1) exhibit both  $p_x$  and  $p_y$  orbitals. However, in contrast to the lattice in Fig. 1, the edge sites (2 and 3) exhibit only the  $p_x$ - (2) or the  $p_y$ -like (3) state in the bonding direction at this energy. Indeed, the additional CO molecules in this design shift the dangling orbital perpendicular to this direction [ $p_y$ -like for site (2) and  $p_x$ -like for site (3)] to much higher energy. Figure 2(b) presents the corresponding LDOS calculated using the muffin-tin model. The nodal character is in excellent agreement with the experimental data. From

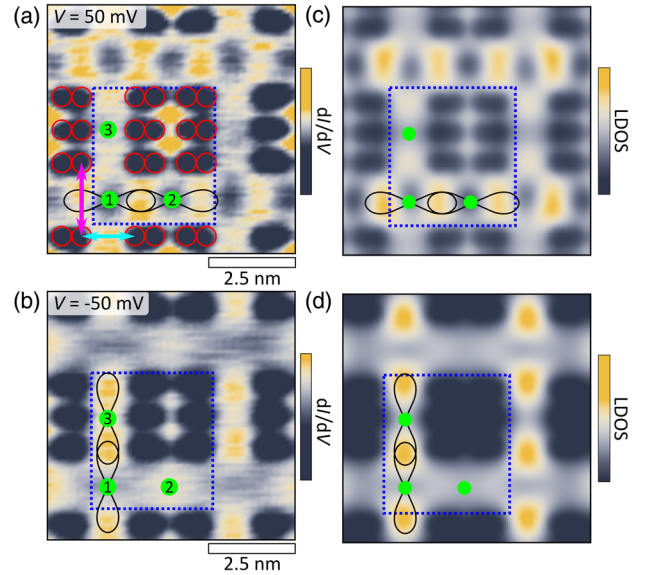


FIG. 3. (a),(b) Differential-conductance maps acquired at  $V = +50$  mV and  $V = -50$  mV, respectively, above an asymmetric Lieb-like lattice with more spacing in the *y* direction (pink arrow) than in the *x* direction (cyan arrow). A part of the lattice is shown. The maps were acquired after stabilization at  $I_{\text{set}} = 1$  nA,  $V_{\text{set}} = +50$  and  $-50$  mV, respectively, with a bias modulation  $V_{\text{rms}} = 5$  mV. (c),(d) Same as (a),(b), calculated using the muffin-tin model.

the muffin-tin results, the wave-function amplitudes can again be extracted, corroborating the  $p$ -like character of the wave functions (see SM [40]). Thus, by tailoring the design, it is possible to have only  $p_x$ -like orbitals on one site and  $p_y$ -like orbitals on another at a given energy.

We now turn our attention to lifting the energy degeneracy of the  $p_x$ - and  $p_y$ -like orbitals at all sites by introducing an asymmetry in the lattice sites [43]. Specifically, we break the fourfold rotational symmetry by increasing the width of artificial-atom sites 1 and 2 in the  $y$  direction by  $\sqrt{3}a$  [pink arrow in Fig. 3(a)] while the  $x$  direction remains the same (cyan arrow). This results in a unit-cell size of  $14a \times 9\sqrt{3}a \approx 3.58 \times 3.99 \text{ nm}^2$ . Figures 3(a) and 3(b) show differential-conductance maps of the asymmetric lattice at  $+50$  and  $-50$  mV, respectively. At  $+50$  mV, we only observe the  $p_x$ -like orbitals [Fig. 3(a)]. In contrast, at  $-50$  mV, only  $p_y$ -like orbitals contribute to the image contrast [Fig. 3(b)]. This can be ascribed to the larger amount of space and therefore reduced confinement in the  $y$  direction. The energy splitting can be considered as an artificial-lattice analogue of crystal-field splitting in solid-state materials. The measurements are reproduced by muffin-tin calculations [see Figs. 3(c) and 3(d) and the SM [40]]. Note that at  $-50$  mV, we observe a

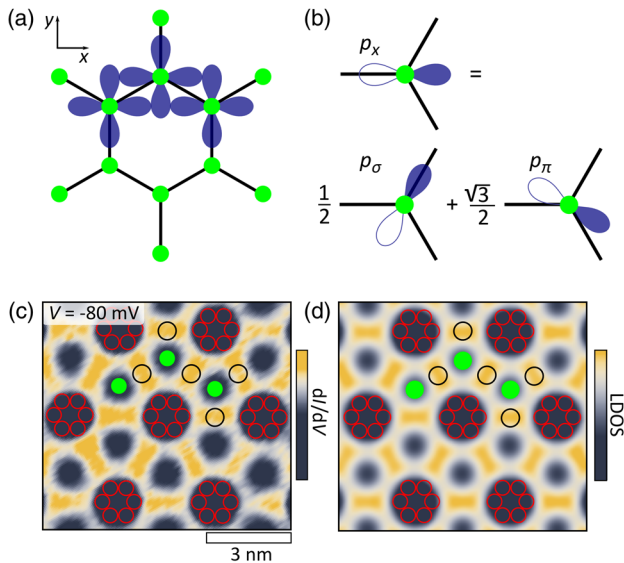


FIG. 4. (a) Schematic of  $p$  orbitals (blue) in a honeycomb arrangement of artificial-atom sites (green). (b) Decomposition of a  $p_x$  orbital into a  $\sigma$  and  $\pi$  bond. The rotation  $\cos(60^\circ) = 1/2$  and  $\cos(-30^\circ) = \sqrt{3}/2$  give the prefactors for these rotations, respectively. (c) Differential-conductance map acquired at  $V = -80$  mV above a honeycomb lattice, shown for a part of the lattice. Several artificial-atom sites (green), the  $\sigma$ -bond overlap of the  $p$ -like orbitals (black contours), and CO molecules (red contours) are indicated. The map was acquired at  $-6$  pm with respect to the set point  $I_{\text{set}} = 1$  nA,  $V_{\text{set}} = 150$  mV, with a bias modulation  $V_{\text{rms}} = 10$  mV. (d) The corresponding LDOS map simulated using the muffin-tin model.

contribution of the  $s$  orbitals at sites 2 and 3 in addition to  $p_y$  orbitals at sites 1 and 3.

We will now extend the approach to a lattice with a threefold rotational symmetry about each artificial-atom site: the honeycomb lattice. Figure 4(a) shows a schematic of a honeycomb lattice. To describe bonding between real atoms in such a geometry typically  $sp^2$  hybridization is invoked. However, because the energy spacing between the  $s$ - and  $p$ -like orbitals in artificial lattices can be made large, orbital hybridization does not necessarily occur in these systems. In this case, a well-established decomposition of the  $p_x$ -like and  $p_y$ -like orbitals into  $\sigma$ - and  $\pi$ -type components can be used to describe the electron localization due to  $p$ -like orbitals in a triangular symmetry [44]. An example of a decomposition of a  $p_x$ -like orbital in a  $\sigma$  and  $\pi$  component is indicated in Fig. 4(b). This leads to increased density of states in between the coupled artificial atoms and nodes at those sites. Figure 4(c) shows a differential-conductance map of the as-such realized honeycomb lattice acquired at  $V = -80$  mV. The artificial-atom sites are indicated in green and the CO molecules are encircled in red (distance between centers of CO clusters is  $14a$ ). The LDOS is highest at locations in between the artificial atoms (black contours), as expected from overlapping  $p$ -type orbitals with a  $\sigma$  bond. The experimental observations are well reproduced by muffin-tin calculations [Fig. 4(d)]. Note that since the decomposition method mentioned above can be used for any lattice symmetry, the  $p$ -like orbital description is expected to be generally applicable.

In conclusion, we demonstrate how to manipulate  $p$ -orbital bands in artificial electronic lattices with fourfold and threefold rotational symmetry. In particular, we show how the  $p_x$  and  $p_y$  orbitals can be tailored spatially and how the energy degeneracy of these states can be lifted, thus creating an analogue of the crystal-field splitting in these artificial lattices. We expect that the approach outlined here can be transferred to lattices created lithographically in semiconductors [45]. The tunability of the geometries towards spherical structures [46] would facilitate adding a well-defined orbital angular momentum to the electrons, offering a platform for the investigation of  $p$ -orbital bands with spin-orbit coupling and their interaction with external fields.

I. S., D. V., and C. M. S. acknowledge funding from NWO via Grants No. 16PR3245, No. DDC 13, and No. 68047534, as well as an ERC Advanced Grant “FIRSTSTEP” 692691. A. A. K. acknowledges funding from NWO via VIDI Grant No. 680-47-534.

[1] Y. Tokura and N. Nagaosa, *Orbital Physics in Transition-Metal Oxides*, *Science* **288**, 462 (2000).

- [2] C. Wu, D. Bergman, L. Balents, and S. Das Sarma, *Flat Bands and Wigner Crystallization in the Honeycomb Optical Lattice*, *Phys. Rev. Lett.* **99**, 070401 (2007).
- [3] C. Wu and S. Das Sarma,  *$p_{x,y}$ -Orbital Counterpart of Graphene: Cold Atoms in the Honeycomb Optical Lattice*, *Phys. Rev. B* **77**, 235107 (2008).
- [4] W. Beugeling, E. Kalesaki, C. Delerue, Y.-M. Niquet, D. Vanmaekelbergh, and C. Morais Smith, *Topological States in Multi-Orbital HgTe Honeycomb Lattices*, *Nat. Commun.* **6**, 6316 (2015).
- [5] G. Wirth, M. Ölschläger, and A. Hemmerich, *Evidence for Orbital Superfluidity in the  $p$ -Band of a Bipartite Optical Square Lattice*, *Nat. Phys.* **7**, 147 (2011).
- [6] M. Ölschläger, G. Wirth, T. Kock, and A. Hemmerich, *Topologically Induced Avoided Band Crossing in an Optical Checkerboard Lattice*, *Phys. Rev. Lett.* **108**, 075302 (2012).
- [7] T. Müller, S. Fölling, A. Widera, and I. Bloch, *State Preparation and Dynamics of Ultracold Atoms in Higher Lattice Orbitals*, *Phys. Rev. Lett.* **99**, 200405 (2007).
- [8] M. Ölschläger, T. Kock, G. Wirth, A. Ewerbeck, C. Morais Smith, and A. Hemmerich, *Interaction-Induced Chiral  $p_x \pm ip_y$  Superfluid Order of Bosons in an Optical Lattice*, *New J. Phys.* **15**, 083041 (2013).
- [9] J. R. Kirtley, C. C. Tsuei, J. Z. Sun, C. C. Chi, L. S. Yu-Jahnes, A. Gupta, M. Rupp, and M. B. Ketchen, *Symmetry of the Order Parameter in the High- $T_c$  Superconductor  $\text{YBa}_2\text{Cu}_3\text{O}_{7-\delta}$* , *Nature (London)* **373**, 225 (1995).
- [10] Y. Maeno, H. Hashimoto, K. Yoshida, S. Nishizaki, T. Fujita, J. G. Bednorz, and F. Lichtenberg, *Superconductivity in a Layered Perovskite without Copper*, *Nature (London)* **372**, 532 (1994).
- [11] A. P. Mackenzie, T. Scaffidi, C. W. Hicks, and Y. Maeno, *Even Odder after Twenty-Three Years: The Superconducting Order Parameter Puzzle of  $\text{Sr}_2\text{RuO}_4$* , *npj Quantum Mater.* **2**, 40 (2017).
- [12] T. Kvorning, T. H. Hansson, A. Quelle, and C. Morais Smith, *Proposed Spontaneous Generation of Magnetic Fields by Curved Layers of a Chiral Superconductor*, *Phys. Rev. Lett.* **120**, 217002 (2018).
- [13] T. Kock, C. Hippler, A. Ewerbeck, and A. Hemmerich, *Orbital Optical Lattices with Bosons*, *J. Phys. B* **49**, 042001 (2016).
- [14] X. Li and W. V. Liu, *Physics of Higher Orbital Bands in Optical Lattices: A Review*, *Rep. Prog. Phys.* **79**, 116401 (2016).
- [15] M. Lewenstein and W. V. Liu, *Optical Lattices: Orbital Dance*, *Nat. Phys.* **7**, 101 (2011).
- [16] M. Milićević, T. Ozawa, G. Montambaux, I. Carusotto, E. Galopin, A. Lemaître, L. Le Gratiet, I. Sagnes, J. Bloch, and A. Amo, *Orbital Edge States in a Photonic Honeycomb Lattice*, *Phys. Rev. Lett.* **118**, 107403 (2017).
- [17] C. Cantillano, S. Mukherjee, L. Morales-Inostroza, B. Real, G. Cceres-Aravena, C. Hermann-Avigliano, R. R. Thomson, and R. A. Vicencio, *Observation of Localized Ground and Excited Orbitals in Graphene Photonic Ribbons*, *New J. Phys.* **20**, 033028 (2018).
- [18] T. Jacqmin, I. Carusotto, I. Sagnes, M. Abbarchi, D. D. Solnyshkov, G. Malpuech, E. Galopin, A. Lemaître, J. Bloch, and A. Amo, *Direct Observation of Dirac Cones and a Flatband in a Honeycomb Lattice for Polaritons*, *Phys. Rev. Lett.* **112**, 116402 (2014).
- [19] S. Klembt, T. H. Harder, O. A. Egorov, K. Winkler, H. Suchomel, J. Beierlein, M. Emmerling, C. Schneider, and S. Höfling, *Polariton Condensation in  $s$ - and  $p$ -Flatbands in a Two-Dimensional Lieb Lattice*, *Appl. Phys. Lett.* **111**, 231102 (2017).
- [20] C. E. Whittaker, E. Cancellieri, P. M. Walker, D. R. Gulevich, H. Schomerus, D. Vaitiekus, B. Royall, D. M. Whittaker, E. Clarke, I. V. Iorsh, I. A. Shelykh, M. S. Skolnick, and D. N. Krizhanovskii, *Exciton Polaritons in a Two-Dimensional Lieb Lattice with Spin-Orbit Coupling*, *Phys. Rev. Lett.* **120**, 097401 (2018).
- [21] N. Nilius, T. M. Wallis, and W. Ho, *Development of One-Dimensional Band Structure in Artificial Gold Chains*, *Science* **297**, 1853 (2002).
- [22] N. Nilius, T. M. Wallis, M. Persson, and W. Ho, *Interplay between Electronic Properties and Interatomic Spacing in Artificial Gold Chains on  $\text{NiAl}(110)$* , *J. Phys. Chem. C* **118**, 29001 (2014).
- [23] S. Fölsch, P. Hyldgaard, R. Koch, and K. H. Ploog, *Quantum Confinement in Monatomic Cu Chains on Cu (111)*, *J. Phys. Chem. C* **118**, 29001 (2014).
- [24] C. F. Hirjibehedin, C. P. Lutz, and A. J. Heinrich, *Spin Coupling in Engineered Atomic Structures*, *Science* **312**, 1021 (2006).
- [25] A. A. Khajetoorians, J. Wiebe, B. Chilian, S. Lounis, S. Blügel, and R. Wiesendanger, *Atom-by-Atom Engineering and Magnetometry of Tailored Nanomagnets*, *Nat. Phys.* **8**, 497 (2012).
- [26] A. Kamlapure, L. Cornils, J. Wiebe, and R. Wiesendanger, *Engineering the Spin Couplings in Atomically Crafted Spin Chains on an Elemental Superconductor*, *Nat. Commun.* **9**, 3253 (2018).
- [27] K. K. Gomes, W. Mar, W. Ko, F. Guinea, and H. C. Manoharan, *Designer Dirac Fermions and Topological Phases in Molecular Graphene*, *Nature (London)* **483**, 306 (2012).
- [28] R. Drost, T. Ojanen, A. Harju, and P. Liljeroth, *Topological States in Engineered Atomic Lattices*, *Nat. Phys.* **13**, 668 (2017).
- [29] M. R. Slot, T. S. Gardenier, P. H. Jacobse, G. C. P. van Miert, S. N. Kempkes, S. J. M. Zevenhuizen, C. Morais Smith, D. Vanmaekelbergh, and I. Swart, *Experimental Realization and Characterization of an Electronic Lieb Lattice*, *Nat. Phys.* **13**, 672 (2017).
- [30] J. Girovsky, J. L. Lado, F. E. Kalf, E. Fahrenfort, L. J. J. M. Peters, J. Fernandez-Rossier, and A. F. Otte, *Emergence of Quasiparticle Bloch States in Artificial Crystals Crafted Atom-by-Atom*, *SciPost Phys.* **2**, 020 (2017).
- [31] L. C. Collins, T. G. Witte, R. Silverman, D. B. Green, and K. K. Gomes, *Imaging Quasiperiodic Electronic States in a Synthetic Penrose Tiling*, *Nat. Commun.* **8**, 15961 (2017).
- [32] S. N. Kempkes, M. R. Slot, S. E. Freney, S. J. M. Zevenhuizen, D. Vanmaekelbergh, I. Swart, and C. Morais Smith, *Design and Characterization of Electrons in a Fractal Geometry*, *Nat. Phys.*, doi: 10.1038/s41567-018-0328-0 (2018).

- [33] M. N. Huda, S. Kezilebieke, T. Ojanen, R. Drost, and P. Liljeroth, *Tunable Topological Domain Wall States in Engineered Atomic Chains*, [arXiv:1806.08614](https://arxiv.org/abs/1806.08614).
- [34] L. Ma, W.-X. Qiu, J.-T. Lü, and J.-H. Gao, *Orbital Degree of Freedom in Artificial Electron Lattices on Metal Surface*, [arXiv:1707.04756](https://arxiv.org/abs/1707.04756).
- [35] S. Paavilainen, M. Ropo, J. Nieminen, J. Akola, and E. Räsänen, *Coexisting Honeycomb and Kagome Characteristics in the Electronic Band Structure of Molecular Graphene*, *Nano Lett.* **16**, 3519 (2016).
- [36] J. A. Stroscio and D. M. Eigler, *Atomic and Molecular Manipulation with the Scanning Tunneling Microscope*, *Science* **254**, 1319 (1991).
- [37] L. Bartels, G. Meyer, and K.-H. Rieder, *Basic Steps of Lateral Manipulation of Single Atoms and Diatomic Clusters with a Scanning Tunneling Microscope Tip*, *Phys. Rev. Lett.* **79**, 697 (1997).
- [38] R. J. Celotta, S. B. Balakirsky, A. P. Fein, F. M. Hess, G. M. Rutter, and J. A. Stroscio, *Invited Article: Autonomous Assembly of Atomically Perfect Nanostructures Using a Scanning Tunneling Microscope*, *Rev. Sci. Instrum.* **85**, 121301 (2014).
- [39] C.-H. Park and S. G. Louie, *Making Massless Dirac Fermions from a Patterned Two-Dimensional Electron Gas*, *Nano Lett.* **9**, 1793 (2009).
- [40] See Supplemental Material at <http://link.aps.org/supplemental/10.1103/PhysRevX.9.011009> for the design of the lattices, local density of states measurements, and for details about the muffin-tin and tight-binding calculations.
- [41] C. Weeks and M. Franz, *Topological Insulators on the Lieb and Perovskite Lattices*, *Phys. Rev. B* **82**, 085310 (2010).
- [42] W.-X. Qiu, S. Li, J.-H. Gao, Y. Zhou, and F.-C. Zhang, *Designing an Artificial Lieb Lattice on a Metal Surface*, *Phys. Rev. B* **94**, 241409 (2016).
- [43] N. Menezes, C. Morais Smith, and G. Palumbo, *Chern-Simons Theory and Atypical Hall Conductivity in the Varma Phase*, *Phys. Rev. B* **97**, 075135 (2018).
- [44] R. Saito, G. Dresselhaus, and M. S. Dresselhaus, *Physical Properties of Carbon Nanotubes* (Imperial College Press, London, 1998).
- [45] A. Tadjine, G. Allan, and C. Delerue, *From Lattice Hamiltonians to Tunable Band Structures by Lithographic Design*, *Phys. Rev. B* **94**, 075441 (2016).
- [46] M. F. Crommie, C. P. Lutz, and D. M. Eigler, *Confinement of Electrons to Quantum Corrals on a Metal Surface*, *Science* **262**, 218 (1993).